Journal of Neurochemistry, 2003, **87**, 1284–1295 doi:10.1046/j.1471-4159.2003.02109.x

Real-time decoding of dopamine concentration changes in the caudate–putamen during tonic and phasic firing

B. Jill Venton,* Hui Zhang,‡ Paul A. Garris,§ Paul E. M. Phillips,*,† David Sulzer‡ and R. Mark Wightman*

*Department of Chemistry and Neuroscience Center and †Department of Psychology, University of North Carolina, Chapel Hill, North Carolina, USA

‡Departments of Neurology and Psychiatry, Columbia University, New York, New York, USA

§Department of Biological Sciences, Illinois State University, Normal, Illinois, USA

Abstract

The fundamental process that underlies volume transmission in the brain is the extracellular diffusion of neurotransmitters from release sites to distal target cells. Dopaminergic neurons display a range of activity states, from low-frequency tonic firing to bursts of high-frequency action potentials (phasic firing). However, it is not clear how this activity affects volume transmission on a subsecond time scale. To evaluate this, we developed a finite-difference model that predicts the lifetime and diffusion of dopamine in brain tissue. We first used this model to decode *in vivo* amperometric measurements of electrically evoked dopamine, and obtained rate constants for release and uptake as well as the extent of diffusion. Accurate predictions were made under a variety of conditions including different regions, different stimulation parameters and with uptake inhibited. Second, we used the decoded rate constants to predict how heterogeneity of dopamine release and uptake sites would affect dopamine concentration fluctuations during different activity states in the absence of an electrode. These simulations show that synchronous phasic firing can produce spatially and temporally heterogeneous concentration profiles whereas asynchronous tonic firing elicits uniform, steady-state dopamine concentrations.

Keywords: amperometry, caudate–putamen, cocaine, diffusion, steady state, volume transmission.

J. Neurochem. (2003) **87,** 1284–1295.

Dopaminergic neurons fire in a low-frequency tonic mode and periodically exhibit bursts of high-frequency action potentials (Wightman and Robinson 2002). Microdialysis studies have revealed that tonic dopamine concentrations are in the low nanomolar range (Justice 1993). Recently, naturally occuring increases in dopamine concentration have been detected on a subsecond time scale with carbon-fiber electrodes (Robinson *et al*. 2002; Phillips *et al*. 2003). These transients appear to arise from phasic firing because they are mimicked by high-frequency electrical stimulation of dopaminergic cell bodies. Like the phasic firing of dopaminergic neurons that occurs during salient stimuli (Schultz 1998), the dopamine transients can be matched to specific behaviors such as interaction with another animal (Robinson *et al*. 2001, 2002) or lever pressing to self-administer cocaine (Phillips *et al*. 2003).

It is well documented that dopamine in the striatum communicates via volume transmission (Garris *et al*. 1994) which differs from the classic synaptic mode of wiring transmission because neurotransmitter can diffuse to target cells distant from release sites (Zoli *et al*. 1998; Vizi 2000). The existence of naturally occuring dopamine concentration transients in the brain raises several questions. Are there temporal differences in dopamine concentrations at release and target sites? Is dopamine volume transmission differentially affected by tonic and phasic firing patterns? To answer such questions, mathematical models that consider the rates of release, uptake and coupled diffusion are required. Although several models have been developed (Nicholson

Received June 10, 2003; revised manuscript received August 27, 2003; accepted August 28, 2003.

Address correspondence and reprint requests to R. Mark Wightman, CB 3290 Venable Hall, Chapel Hill, NC 27599-3290, USA.
E-mail: rmw@unc.edu

Abbreviations used: BAN, basolateral amygdaloid nucleus, CP, caudate–putamen, DAT, dopamine transporter, DOQ, dopamine-*o*-quinone; GAD, glutamic acid decarboxylase, PBS, phosphate-buffered saline; SN/VTA, substantia nigra/ventral tegmental area.

1995; Cragg *et al*. 2001; Schmitz *et al*. 2001; Schönfuß *et al*. 2001), they have been used only to model exogenous dopamine or stimulated release, and have not been extended to make neurochemical predictions.

In this work, we adapted the models of Schmitz *et al*. (2001) and Schönfuß *et al*. (2001) to address these questions about dopamine volume transmission. Amperometric detection was used because of its high temporal resolution. We fitted the model to *in vivo* amperometric recordings of electrically evoked dopamine transients obtained in the brain of anesthetized rats. The fitting allowed decoding of regionally specific rate constants for dopamine release and uptake as well as the apparent diffusion distance of dopamine from release sites to the electrode. In addition we evaluated the effects of inhibition of the dopamine transporter (DAT) by cocaine and nomifensine. Having established the validity of the model in describing experimental data, we next used it to predict extracellular dopamine signaling during phasic and tonic firing patterns in the absence of any measurement perturbations. We found that a heterogeneous distribution of uptake and release sites causes striking variations in local dopamine concentrations during synchronous phasic firing. In contrast, we determined that asynchronous, low-frequency tonic firing produces a steady-state concentration even on the millisecond time scale.

Materials and methods

Electrochemistry

Cylinder microelectrodes were fabricated by sealing a 5-μm diameter T-650 carbon fiber (Thornel, Amoco Co., Greenville, SC, USA) in a pulled glass capillary (Cahill *et al*. 1996). The fiber was cut so that 40–50 μm protruded from the end. Electrodes were epoxied (Miller-Stevenson, Danbury, CT, USA) to ensure a good seal, and dipped immediately in acetone for a few seconds to remove residual epoxy from the carbon fiber. All electrodes were soaked overnight in isopropanol purified with activated carbon (Norit A; ICN Biomedicals, Aurora, OH, USA) before use (Bath *et al*. 2000).

For dopamine detection with cyclic voltammetry, the electrode was held at − 0.4 V and scanned to 1.0 V and back at 300 V/s every 100 ms (Michael *et al*. 1999). For amperometry, the electrode was held at + 0.3 V versus Ag/AgCl and the collection frequency was 60 Hz (Venton *et al*. 2002). A computer-generated waveform was sent to a patch clamp amplifier (Axopatch 200B; Axon instruments, Foster City, CA, USA), in whole-cell mode, modified for use in electrochemical measurements. Data were collected through an acquisition board (PCI-MIO-16E-10; National Instruments, Austin, TX, USA) interfaced with a computer. A timing board was used to synchronize electrical stimulations with data acquisition. Amperometry yielded better signal-to-noise ratios than cyclic voltammetry. The average signal-to-noise ratio for a 24-pulse, 60-Hz stimulation with amperometry was 71 ± 7 which was significantly greater than that for cyclic voltammetry, 51 ± 6 ($p < 0.05$, $n = 11$ animals).

Electrodes were calibrated using a flow injection analysis system described previously (Kristensen *et al*. 1986). Buffer containing 20 mM HEPES, 150 mM NaCl, 1.2 mM $CaCl_2$ and 600 μM ascorbate, adjusted to pH 7.4, was used in all calibrations (Venton *et al*. 2002). This high concentration of ascorbate is necessary in order for calculated concentrations from calibrations of cyclic voltammetry and amperometric data to agree. All chemicals were used as received from Sigma-Aldrich (St Louis, MO, USA). Aqueous solutions were prepared using double-distilled deionized water (Megapure System; Corning Model D2, Corning, NY, USA).

Animal and surgical procedures

Male Sprague–Dawley rats (275–350 g; Charles River, Wilmington, MA, USA) were anesthetized with urethane (1.5 g/kg, i.p.). Core body temperature was maintained by placing the animal on a Deltaphase isothermal pad (Braintree Scientific, Braintree, MA, USA). For some studies, a hole was drilled in the skull for the placement of the carbon-fiber microelectrode in the caudate–putamen (CP) (stereotaxic coordinates, in millimetres from bregma, anterior-posterior (AP), + 1.2; medial-lateral (ML), + 2.0; dorsal-ventral (DV), − 4.5 from dura) (Paxinos and Watson 1986). In other experiments in which the CP and the basolateral amygdaloid nucleus (BAN) were compared, a hole was drilled in the skull at AP − 2.3, ML + 4.5 and the carbon-fiber microelectrode was lowered to about − 5.0 for the CP and about −8.2 for the BAN. For all experiments, the bipolar stimulating electrode (Plastics One, Roanoke, VA, USA) was placed in the substantia nigra/ventral tegmental area (SN/VTA) region (AP, − 5.6; ML, + 1.0; DV, − 7.5). The dorsoventral placement of the stimulating electrode was adjusted to maximize dopamine efflux. The circular tips of the stimulating electrode were polished before the experiment, separated so that they were about 1 mm apart, and inserted with both tips perpendicular to the midline. Four biphasic stimulating pulses, 2 ms long, 300 μA of constant current each phase, were applied at 100 Hz unless otherwise indicated. This stimulation protocol promotes transient release that allows diffusional delays to be more apparent. A Ag/AgCl wire was also implanted in the brain as a reference electrode.

Drugs

Cocaine (10 mg/kg, i.p.) and nomifensine (7 mg/kg, i.p.) were purchased from Sigma (St Louis, MO, USA) and dissolved in 1 ml saline. Ten milligrams of tartaric acid was used to help dissolve nomifensine. For control experiments, 1 ml of saline was injected (i.p.).

Antibody labeling of slices

Mice used in this study were 8-week-old male C57BL/6 mice from Jackson Laboratory (Bar Harbor, ME, USA). All mice were anesthetized (pentobarbital, 30 mg/kg i.p.) and perfused intracardially with 25 mL normal saline followed by 75 mL 4% (w/v) paraformaldehyde in 0.1 M phosphate buffer (4% PF/PB, pH 7.1). Brains were then dissected out, postfixed by immersion in 4% PF/PB (2 h, 4°C), cryoprotected in 30% (w/v) sucrose in phosphate buffer, and frozen by immersion in isopentane cooled on dry ice. Frozen brain samples were cut (30 μm) coronally in a cryostat. The sections were collected in ice-cold phosphate buffer free floating, and then successively rinsed (three times each for 5 min) in phosphate-buffered saline (PBS), blocked in 10% normal goat serum in PBS containing 0.1% Triton X-100 (60 min, 25°C), and incubated with anti-rabbit glutamic acid decarboxylase (GAD)

65/67 (1 : 500; Sigma) and anti-rat DAT (1 : 200; Chemicon, Temecula, CA, USA) containing 2% normal serum (24 h, 4°C). Antibody deposits were then detected by incubation for 30 min at 25°C in PBS with goat anti-rabbit IgG conjugated to tetramethyl rhodamine isothiocyanate (TRITC) (1 : 200; Sigma) and goat anti-rat IgG conjugated to fluorescein isothiocyanate (FITC) (1 : 200; Sigma). The sections were then washed five times each for 10 min, mounted and visualized with a confocal laser microscope.

Statistical analysis

Drug effects and regional differences in diffusion were evaluated statistically using paired *t*-tests in Microsoft Excel. Data were considered significant at the 95% confidence level and are reported as the mean ± SEM for *n* animals. The finite-difference model of diffusion is described in detail in the Appendix. Model parameters were evaluated by visually comparing experimental data and simulated curves.

Results

Characteristics of the model

Simulating the dopamine response

The instantaneous dopamine concentration in the extracellular space is determined by the rates of release, uptake and mass transport (Nicholson 1995). Amperometry detects these dynamics via oxidation of dopamine (Dugast *et al*. 1994), and the dopamine-*o*-quinone (DOQ) generated is subsequently reduced by the high concentration of extracellular ascorbate (the catalytic reaction; Venton *et al*. 2002). Simulations of amperometric dopamine detection that account for these factors are shown in Fig. 1 during release evoked by a burst of four pulses at 100 Hz (see Appendix for description of the model). When dopamine release and uptake sites extend to the electrode (Fig. 1a), the modeled amperometric response shows that dopamine would be detected immediately with each stimulation pulse and decay after the end of stimulation (Fig. 1b). In this situation there are no concentration gradients so diffusion does not affect the result. However, if a region that contains uptake sites, but not release sites, is placed between the electrode and a region of spatially uniform release and uptake sites (Fig. 1c), a delay in the amperometric response is seen. The region adjacent to the electrode, termed the apparent diffusion distance (length d_{app}), includes uptake sites to be consistent with previous models (Schmitz *et al*. 2001; Schönfuß *et al*. 2001). If the effect of the catalytic reaction of DOQ and ascorbic acid is neglected (Venton *et al*. 2002), a shorter time to peak following cessation of stimulation (indicated by the horizontal bracket) would be erroneously predicted (Fig. 1d).

Release sites are expected to be distributed over a range of distances from the cylindrical electrode because its length (~ 50 μm) is much greater than the mean distance between sites (Doucet *et al*. 1986). To examine how this spatial heterogeneity would affect the apparent diffusion distance, we modeled a simple case in which half of the electrode was

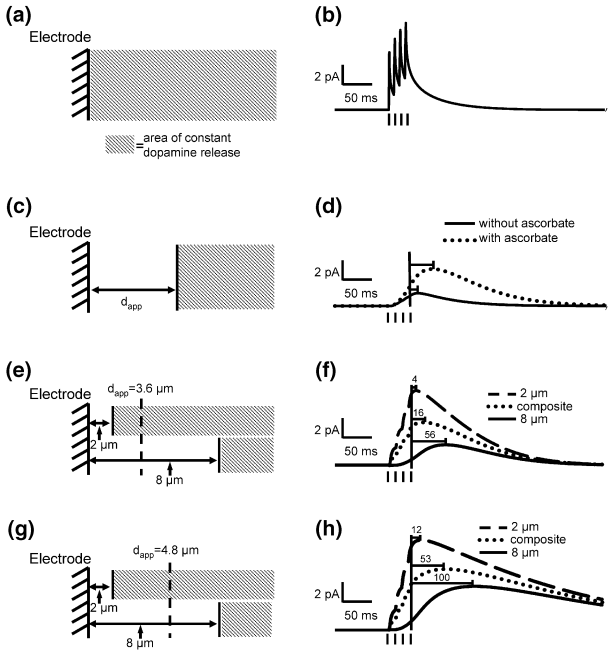

Fig. 1 Finite-difference diffusion model. All amperometry current traces were generated for the kinetic parameters $[DA]_p = 0.1$ μM, $K_m = 0.2$ μM, $V_{max} = 4.0$ μM/s and $d_{app} = 5$ μm unless noted otherwise. (a) Schematic of release sites extending to the electrode ($d_{app} = 0$). The shaded area represents the modeled area of constant release. (b) Finite-difference model of dopamine concentrations during a four-pulse (100 Hz) stimulation (vertical lines under plot) for the case in (a). (c) Schematic of the arrangement of sites when an apparent diffusion distance (d_{app}) is included in the model. (d) The solid line is a simulation for the geometry of Fig. 1(c) without accounting for the effects of ascorbate and the dotted line is a simulation accounting for the catalytic reaction of ascorbate to regenerate dopamine. (e) A configuration representing two populations of closest release sites. The dashed line shows the apparent diffusion distance calculated by fitting the average of the 2- and 8-μm curves from Fig. 1(f). (f) Modeled response to a four-pulse, 100 Hz stimulation with a d_{app} of 2 μm (dashed line) and 8 μm (solid line). The dotted line is the average of two curves and corresponds to a d_{app} of 3.6 μm. The time to peak of each curve is labeled in milliseconds. (g) Illustration of the effect of uptake inhibition on the apparent diffusion distance calculated from averaging the traces from two populations of closest release sites. (h) The analysis of Fig. 1(f) was repeated except that K_m was increased to 0.8 μM to simulate uptake inhibition. The time to peak of each curve is labeled in milliseconds. The average trace corresponds to a d_{app} of 4.8 μm.

2 μm from the closest release site and the other half 8 μm away (Fig. 1e). The averaged traces correspond to a simulation with d_{app} of 3.6 μm. The apparent diffusion distance is smaller than the arithmetic mean of the d_{app} values because the closest site contributes more. For this reason we use the term 'apparent' diffusion distance rather than average distance as used elsewhere (Schönfuß *et al*. 2001). The range of distances of contributing release sites from the electrode cannot be determined from a single amperometric

curve. For this reason, the modeling of experimental data leads to a singular value of d_{app} even though release sites are spatially disperse. In Figs 1(g) and (h) we evaluated the same spatial heterogeneity, but with K_m increased to 0.8 μM to mimic uptake inhibition. This increased the delay in the time to peak and the apparent diffusion distance for the average increased to 4.8 μm. Uptake inhibition allows sites further away to contribute more dopamine to the electrode, increasing the apparent diffusion distance.

Spatial profiles of dopamine concentrations can also be simulated, revealing the perturbation of the dopamine concentration near the electrode caused by the amperometric detection (Figs 2a and b). If ascorbate is neglected (solid line), the concentration gradient of dopamine is approximately linear. However, at physiological ascorbate levels the catalytic reaction maintains the concentration of dopamine near the electrode by recycling the *o*-quinone back to dopamine. The electro-oxidation does not affect the dopamine concentration at distances beyond 30 μm, where it is regulated only by uptake and release.

Features revealed by the model

The simulation of the *in vivo* amperometric responses reveals three important factors. First, if release sites are located a finite distance away from the electrode there will be a delay between the end of the stimulation and the maximal signal. Second, the duration of this delay will be determined by the proximity of release sites. Third, this delay should increase after competitive uptake inhibition because of a greater contribution of diffusion from distal release sites. These predicted features were tested to verify that the model accurately described *in vivo* data.

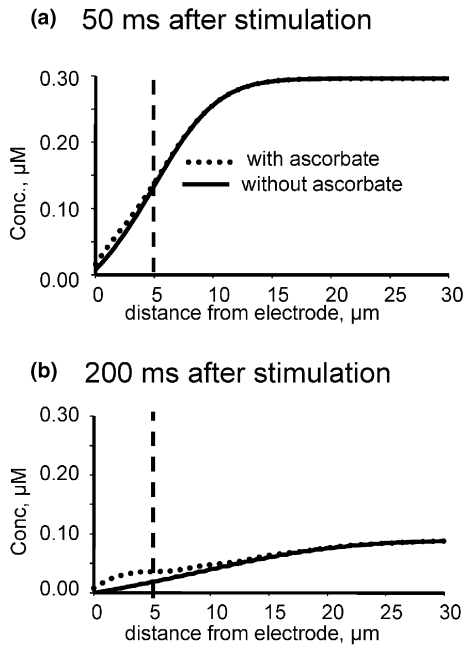

Fig. 2 Spatial profiles of dopamine concentrations during simulated amperometry. Concentration versus distance profile for the model with (dots) and without (solid line) the catalytic reaction of ascorbate are shown. The electrode is placed at the origin and the vertical dashed line marks the end of the region without release. The modeled parameters were $[DA]_p = 0.1$ μM, $K_m = 0.2$ μM, $V_{max} = 4.0$ μM/s and $d_{app} = 5$ μm. (a) Dopamine profile 50 ms after stimulation. (b) Concentration profile 200 ms after stimulation.

Testing the model *in vivo*

Evoked release of dopamine

Electrical stimulation of the SN/VTA region evokes dopamine release in various terminal fields in anesthetized rats. In this work, evoked release was initially verified as dopamine with fast-scan cyclic voltammetry and then the evoked dynamics were sampled at high temporal resolution using constant-potential amperometry. The dots in Fig. 3a show an amperometric trace measured in the CP during a four-pulse, 100-Hz stimulation. Note that detectable dopamine flux does not occur until approximately 15 ms after the first stimula-

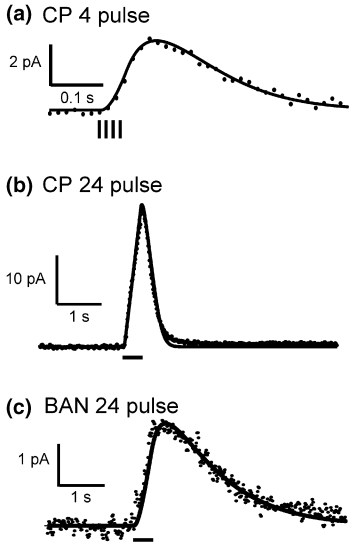

Fig. 3 Comparison of dopamine diffusion in the CP and the BAN. (a) Dopamine release in the CP measured by amperometry during a four-pulse (100 Hz) stimulation (dots). The vertical lines underneath the trace mark the four stimulation pulses. The solid line is the finite-difference model with $[DA]_p = 99$ nM, $K_m = 0.2$ μM, $V_{max} = 4.0$ μM/s and $d_{app} = 5.5$ μm. (b) Electrically evoked (24 pulses, 60 Hz) dopamine measured in the CP (note that a different part of the CP was studied from that in Fig. 3a). The bar under the traces represents the length of the pulse train. The line is the finite-difference model with $[DA]_p = 110$ nM, $K_m = 0.20$ μM, $V_{max} = 3.6$ μM/s and $d_{app} = 5.5$ μm. Note the time scale is different from that in Fig. 3(a). (c) Dopamine efflux in the BAN after a 24-pulse, 60-Hz stimulation of the SN/VTA. Ten amperometric traces taken at 1-min intervals were signal averaged (dots). The modeled data (solid line) are based on $[DA]_p = 8$ nM, $K_m = 0.58$ μM, $V_{max} = 0.53$ μM/s and $d_{app} = 11$ μm.

Table 1 Mean kinetic parameters for dopamine

Parameter	CP (four pulses, 100 Hz)	CP (24 pulses, 60 Hz)	BAN (24 pulses, 60 Hz)
$[DA]_p$ (nM)	160 ± 20	120 ± 20	8 ± 2
K_m (μM)	0.20 ± 0.01	0.23 ± 0.04	0.58 ± 0.08
V_{max} (μM/s)	3.9 ± 0.2	3.8 ± 0.3	0.58 ± 0.08
d_{app} (μm)	6.0 ± 0.5	6.0 ± 0.5	11.5 ± 0.8

Values given were obtained from fitting of the model in case (i), as seen in the Appendix, to experimental data obtained in the regions indicated during stimulation of the SN/VTA region. $[DA]_p$ is the concentration of dopamine that is released into the extracellular fluid with each stimulus pulse, V_{max} is the maximal rate of uptake by the dopamine transporter, and K_m is the affinity of the dopamine transporter for dopamine. The apparent diffusion distance from release sites to the electrode is given by d_{app}. Values are mean ± SEM for $n = 4$ rats (CP 24 pulses and BAN) or $n = 12$ (CP four pulses).

tion pulse (vertical lines) and that the increase in concentration continues after the pulses have terminated, i.e. the delay is present. The average value for this diffusional delay in the time to peak was 65 ± 9 ms in the CP with this stimulation ($n = 12$ animals). The finite-difference model fits well with the *in vivo* amperometric data (case (i) in Appendix; solid line Fig. 3a). Table 1 gives mean kinetic parameters from measurements in the CP of 12 animals.

Comparison of dopamine diffusion in the BAN and CP

Our model predicts that terminal density will affect the amperometric signal because the distance between release sites and the electrode affects the measured apparent diffusion distance. To test this, evoked dopamine release was compared in the CP and the BAN, a region with sparse dopaminergic innervation. The electrode was first lowered into the CP (note this is a more caudal part of the CP than in the previous figure), then through a border region that lacks dopamine input and finally into the BAN (Garris and Wightman 1994b). A longer stimulation, 24 pulses at 60 Hz, was used because of the low release of dopamine in the BAN (Figs 3b and c; note the change in time scale from Fig. 3a). Release and uptake rate constants (Table 1) in each region are distinct as reported previously (Jones *et al*. 1995). In the CP, the time to peak for a 24-pulse stimulation was 83 ± 7 ms, significantly less than the 340 ± 35 ms measured in the BAN ($p < 0.01$, $n = 4$). To account for the longer time to peak, the length of d_{app} had to be increased from 6.0 ± 0.5 μm in the CP to 11.5 ± 0.8 μm in the BAN ($p < 0.01$, $n = 4$). In the CP, both the four-pulse (100 Hz) and 24-pulse (60 Hz) stimulations yielded the same value of d_{app} (Table 1), indicating that d_{app} is independent of the stimulus parameters.

An independent prediction of the difference in d_{app} between brain regions can be made from the dopamine terminal density. Terminal density should be proportional to the dopamine tissue content, which is 90 ng per mg protein in the CP and 15 ng per mg protein in the BAN (Garris and Wightman 1994a), a ratio of 6.0. Alternatively, the site density can be predicted from the number of transporters, which is directly proportional to V_{max}. Consistent with the estimate above, this method gives a ratio for the two regions of 6.7 (Table 1). Taking the cube root of these values gives the ratio of the average distance between release sites, which is 1.8 or 1.9 for each method. The experimentally determined ratio of d_{app} values for the BAN relative to the CP is 1.9 ± 0.2, which agrees remarkably well with both methods of calculation.

Effects of dopamine uptake inhibitors

The prediction of the model that uptake inhibition would cause an increase in d_{app} was also tested by administering the competitive uptake inhibitors cocaine (10 mg/kg i.p.) and nomifensine (7 mg/kg i.p.) (Fig. 4). Fifty minutes after uptake inhibition, the peak height is slightly increased and the rate of disappearance of dopamine is slower. The time to

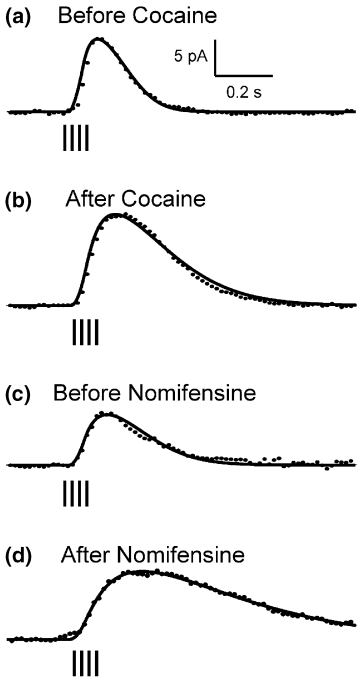

Fig. 4 Effect of uptake inhibitors on the dopamine response. Amperometric (dots) and modeled data (lines) before and 50 min after i.p. administration of cocaine (10 mg/kg) or nomifensine (7 mg/kg). For (a) and (b), V_{max} and $[DA]_p$ were held constant at 5 μM/s and 0.21 μM respectively. (a) Before cocaine, $K_m = 0.20$ μM and $d_{app} = 5.0$ μm. (b) After cocaine, $K_m = 0.61$ μM and $d_{app} = 7.5$ μm. For (c) and (d) V_{max} was kept constant at 3.5 μM/s and $[DA]_p$ at 0.21 μM. (c) Before nomifensine, $K_m = 0.20$ nM and $d_{app} = 6.5$ μm. (d) After nomifensine, $K_m = 0.87$ nM and $d_{app} = 9.0$ μm. The scale bar is the same for all panels.

Table 2 Mean changes in dopamine dynamics after uptake inhibition

	Cocaine (10 mg/kg)	Nomifensine (7 mg/kg)
Increase in time to peak (ms)	150 ± 14*	158 ± 29*
Apparent increase in K_m (% predrug value)	340 ± 65*	400 ± 70*
Increase in d_{app} (μm)	2.5 ± 0.5*	2.8 ± 0.5*

All changes are mean ± SEM for five animals per drug, calculated 50 min after drug administration. *$p < 0.05$ versus predrug value using paired *t*-test.

peak significantly increased from 60 ± 5 ms to 210 ± 13 ms after cocaine ($p < 0.01$, $n = 5$) and from 68 ± 12 ms to 225 ± 27 ms after nomifensine ($p < 0.01$, $n = 5$). In contrast, in animals in which saline was administered as a control there was no change in time to peak, K_m or V_{max} after the same time, but there was a small decrease in the concentration of dopamine released into the extracellular fluid with each stimulus pulse ($[DA]_p$) (to about 85% of the initial value; $n = 4$, data not shown).

Mean changes in the kinetic parameters after uptake inhibition are given in Table 2. V_{max} and $[DA]_p$ were determined from the predrug results and kept constant in the simulations after the drug was given. The K_m for the transporter was set to 0.20 μM before drug administration (Near *et al*. 1988), and was adjusted to fit the data after uptake inhibition. The fits also required an increase in d_{app}, the predicted result following uptake inhibition for a distribution of release site locations (Fig. 1). Extracellular ascorbate concentration can increase by up to 50% following administration of the uptake inhibitors amphetamine or GBR 12909 (Pierce and Rebec 1990). However, simulations with such an increase in ascorbate produce curves that have much shorter time to peak values than are observed. Thus, the catalytic reaction is not responsible for the observed change in the time to peak.

Predictions of dopamine concentration profiles in the absence of an electrode

Effects of uptake and release site heterogeneity on tonic and phasic dopamine release

Once rates for diffusion, uptake and release were established, simulations were made of dopamine dynamics in striatal tissue without the perturbation caused by a sensor (case (ii) in Appendix). Striatal heterogeneity was estimated using an immunostained photomicrograph of mouse CP (Fig. 5a). DAT sites are labeled green and GAD (an enzyme for GABA synthesis) sites are labeled red. To translate the information in the photomicrograph into a form suitable for modeling, a one-dimensional strip was taken and it was assumed that all green areas exhibit dopamine release and uptake ('hot' spots), and that dark areas (on the edge of non-dopaminergic cells) exhibit neither. To account for circuitous diffusion pathways around the cell bodies, the diffusion coefficient was reduced by a tortuosity factor (Nicholson 1995). Neurochemical rates are similar in rats and mice (compare Jones *et al*. 1995 with Jones *et al*. 1999) so we used the kinetic parameters established in the rat brain.

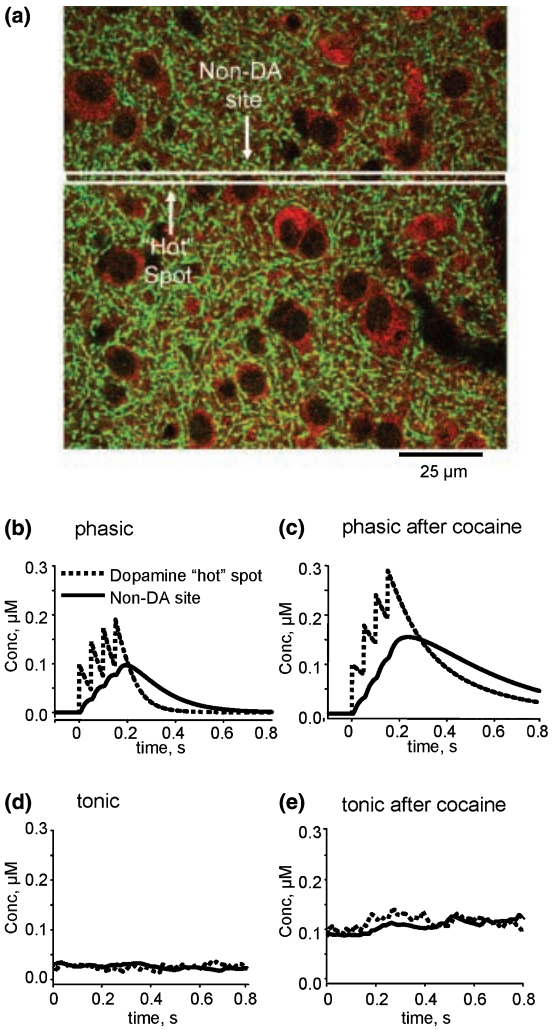

Fig. 5 Model of heterogeneous release and uptake sites in the CP. (a) An immunostained slice of a mouse CP. The dopamine transporter is labeled green and GAD, an enzyme that synthesizes GABA, is labeled red. The box is the section modeled. Examples of a dopamine 'hot' spot, with release and uptake sites, and a non-dopaminergic (non-DA) innervated site, without release and uptake sites, are labeled. In (b–e) the simulation parameters were $[DA]_p = 0.1$ μM, $K_m = 0.2$ μM and $V_{max} = 4.0$ μM/s. The legend is the same for all the graphs. (b) Simulations of dopamine concentration during and after a synchronous four-pulse (20 Hz) phasic burst initiated at time 0 s in a hot spot (dotted line) and near a non-dopaminergic cell body (solid line). (c) Response to phasic firing after uptake inhibition, simulated by an increase in K_m to 0.8 μM. (d) Simulation of dopamine concentration over time for tonic, asynchronous firing at 5 Hz. (e) Tonic firing concentration profiles after uptake inhibition.

The predicted responses to phasic and tonic firing are shown in Figs 5(b–e). Phasic firing was simulated as four synchronized action potentials at 20 Hz, a typical frequency and number of pulses for a burst measured using electrophysiology (Grace 1995; Hyland *et al*. 2002). Low-frequency, asynchronous firing patterns were used to simulate tonic firing, with neurons firing independently of each other at an average rate of 5 Hz (Grace and Bunney 1984; Schultz 1986). In the hot spot, distinct increases in dopamine accompany the action potentials (Fig. 5b). There is no delay in the peak concentration; because of the proximity of release sites and adjacent uptake sites the dopamine is quickly removed. In contrast, when there are no release and uptake sites the maximal concentration is lower and changes are delayed. After uptake inhibition, the maximum concentration in the regions where release occurs during phasic firing is increased and decays more slowly back to baseline (Fig. 5c). In areas without release and uptake sites, however, the concentration changes are delayed because the dopamine must diffuse into the area.

With tonic firing there is a low, steady-state dopamine concentration regardless of the proximity of uptake and release sites (Fig. 5d). After uptake inhibition the concentration remains steady, and increases at both the surface of non-dopaminergic cells and in hot spots (Fig. 5e). These predictions show that, following phasic firing, the dopamine concentration profile that a receptor on a GABAergic cell body would experience is different from that of a receptor near a release site in a hot spot. In contrast, there are no differences in dopamine concentration between hot spots and non-dopaminergic cells for tonic firing.

The spatial distribution of concentrations resulting heterogeneous release and uptake site locations can also be modeled. The concentration profile for dopamine throughout the modeled area is shown for phasic firing at the end of a burst (dotted line) and 100 ms later (solid line) (Fig. 6a). At the end of the burst, the concentration is raised in the innervated regions (green areas) with a lower concentration near the non-dopaminergic cell bodies (dark areas). The concentration profile reverses 100 ms after the burst, with the highest dopamine concentrations appearing in the areas without release and uptake. In contrast, regions with a high amount of DAT show a diminished dopamine concentration at this time. After uptake inhibition, the effects of heterogeneity are more pronounced during the burst but are less evident after the firing ends (Fig. 6b). The lowered uptake rate leaves time for the local concentrations to mix and become more uniform.

In Figs 6(c and d), the colored traces are the concentration profiles for tonic firing at several time points and the black line is the time-averaged concentration. This simulation demonstrates that tonic firing produces an essentially steady-state concentration of dopamine at all times, regardless of the location of release and uptake sites. After uptake inhibition, the concentration profiles are shifted and the basal dopamine level increases from 30 nM to 110 nM.

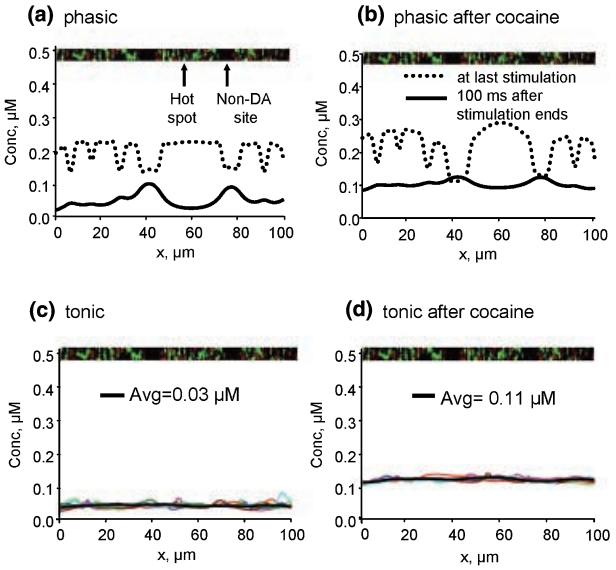

Fig. 6 Simulations of spatially heterogeneous dopamine concentrations during tonic and phasic firing. The *x* axis is distance across the modeled region and the curves represent the concentrations averaged over 2 ms. (a) Dopamine concentration versus distance profiles for a four-pulse, 20-Hz burst are illustrated at two times: at the last impulse (dotted line) and 100 ms after the train (solid line). The simulation parameters are the same as those in Fig. 5. The bar above the graph (taken from the box in Fig. 5a) shows the layout of release and uptake sites. Green areas were assumed to have release and uptake sites, whereas dark areas were assumed to have neither. A hot spot and site without dopaminergic innervation (non-DA) are labeled. (b) Heterogeneous dopamine concentration profiles arise during a burst after uptake inhibition (simulated as a change in K_m to 0.8 μM). (c) The colored traces are the dopamine concentration profiles at different times. The black line is the mean profile (averaged over 2 s) of dopamine during tonic firing. (d) Tonic dopamine concentrations after uptake inhibition. The colored lines represent specific time points and the black line denotes the time-averaged (2 s) concentration of dopamine.

Simultaneous spatial and temporal views of these dynamic events are best represented in a movie. The accompanying supplementary material shows the simulation of release and uptake in the box in Fig. 5(a) for continuous tonic firing and then a phasic burst (at 0.4 s in the movie). From the movie, it is quite clear that tonic firing results in low, uniform dopamine concentrations, whereas phasic firing results in a large, spatially heterogeneous concentration increase.

Discussion

In this paper, a finite-difference model describing dopamine concentrations resulting from dopamine release, uptake and diffusion was evaluated. The model was used to decode the

kinetic values from amperometric measurements, and then to evaluate how heterogeneity of release and uptake site locations affects dopamine concentration profiles elicited by tonic and phasic firing in the absence of an electrode. Despite the heterogeneous distribution of release and uptake sites, tonic firing results in spatially uniform dopamine concentrations that are temporally static. In contrast, synchronous phasic firing results in large temporal and spatial fluctuations that are dramatically affected by this heterogeneity.

Modeling dopamine diffusion in the brain

The first goal of this study was to extract accurate kinetic parameters from the *in vivo* amperometric measurements through the use of an appropriate mathematical model. Amperometry is ideal for measuring the kinetics of dopamine neurotransmission because it has an instantaneous response to dopamine (Suaud-Chagny *et al*. 1995; Venton *et al*. 2002). Electrophysiological results show that, when dopaminergic axons are electrically stimulated, each stimulation pulse generates an action potential and that neuronal firing ends when stimulation is terminated (Kuhr *et al*. 1987). Therefore, the continued rise of the amperometric signal after the end of the stimulation is due to dopamine diffusion in the brain extracellular space and an apparent diffusion distance adjacent to the electrode is necessary to model this. Some tissue adjacent to the electrode may have been damaged during electrode insertion, although preliminary studies suggest that such damage is quite small (Allen *et al*. 2001), especially compared with that caused by a microdialysis probe (Clapp-Lilly *et al*. 1999). Indeed, the sensitivity of d_{app} to uptake inhibition and the density of terminals clearly indicate that the electrode is sampling from viable tissue.

To test the validity of the model, three sets of experiments were performed. First, we varied the stimulus duration from 40 ms to 400 ms at two different frequencies (Fig. 3). This changed the time to peak concentration after stimulation, but there was no change in the extracted d_{app}. This demonstrates that a model is needed to evaluate these results because a change in the time to peak does not necessarily indicate an increase in diffusion. Second, data from the CP were compared with those from the BAN. The apparent diffusion distance was greater in the BAN and the increased distance scaled exactly with that computed from the relative terminal density of the two regions. Third, data were modeled before and after the administration of uptake blockers. Although others have also observed an increase in diffusion distance after uptake inhibition (Schönfuß *et al*. 2001), our simulations reveal how a distribution of release sites at different distances from the electrode leads to an increase in d_{app}. Uptake inhibition simply allows dopamine diffusing from further distances to contribute more to the measured signal.

Previous estimates of diffusion distance in the CP, between 4.5 and 7.0 μm (Gonon *et al*. 2000; Peters and Michael 2000), are quite similar to our value of 6 μm. The appropriate handling of the diffusional aspects allows more accurate estimation of the kinetic rate constants controlling release and uptake. Remarkably, our V_{max}, K_m and $[DA]_p$ values agree with results obtained by cyclic voltammetry at Nafion-coated electrodes (Jones *et al*. 1995), which required correction by deconvolution of the time constant for permeation through the Nafion film. Future models incorporating depression and augmentation of dopamine release by factors such as terminal autoreceptor effects should provide even more elegant predictions of dopamine concentrations.

Effects of striatal heterogeneity on dopamine dynamics during tonic and phasic firing

Once the model was established, simulations were used to address how different firing patterns, and heterogeneity of release and uptake site locations, affect dopamine volume transmission without an electrode present. The CP is a spatially complex organization of neuronal systems. For example, there are patch-matrix compartments that contain different receptors, neurotransmitters, afferents and efferents (Fallon and Moore 1978; Graybiel 1990; Gerfen 1992). There is microscopic heterogeneity in the location of DATs (Nirenberg *et al*. 1996) and dopamine receptors (Sesack *et al*. 1994). In addition, dopamine neurons fire in complex patterns with bursts of action potentials spaced at irregular intervals among tonic firing patterns (Grace 1995). Therefore, we addressed the questions (1) are there temporal differences in dopamine concentrations at release sites and GABAergic cells, and (2) how do tonic and phasic firing patterns affect these concentration profiles?

Quantitative predictions of phasic dopamine dynamics are important because (1) phasic firing occurs in response to salient sensory information (Schultz 1998; Hyland *et al*. 2002); (2) it leads to transiently raised levels (Dugast *et al*. 1994); and (3) these transients are observed in behavioral situations and influence motor output (Robinson *et al*. 2002; Phillips *et al*. 2003). During bursts, multiple dopaminergic neurons fire together owing to gap junctions between them (Grace and Bunney 1983) or common synchronous inputs (Hyland *et al*. 2002). The simulations reveal that dopamine concentrations are dramatically different during phasic firing near non-dopaminergic cell bodies than in 'hot' spots, where dopamine appears instantly owing to release (Fig. 6). Thus, temporally and spatially heterogeneous extracellular dopamine concentrations occur during a burst despite a synchrony in the electrical activity of dopaminergic neurons. Because dopamine receptors have a broad range of affinities, ranging from low nanomolar to micromolar (Richfield *et al*. 1989), these differences in temporal and spatial dynamics during phasic firing support multifunctionality of dopamine signaling at the different receptor subtypes in the terminal region. Thus, although dopamine can act locally at receptors adjacent

to dopamine release sites, the simulations reveal that under burst-firing conditions it can diffuse further leading to high concentrations at remote receptors located far from the release sites.

Although tonic firing is thought to maintain the low basal concentration of extracellular dopamine measured by microdialysis, fluctuations in these levels on a subsecond time scale have not been examined. Tonic firing was simulated by asynchronous firing at low frequencies because there is little experimental evidence for synchronicity during tonic firing. Indeed, because our amperometric measurements have a detection limit of less than 20 nM, the quiet background signal observed supports the assumption of asynchronous firing. Tonic firing leads to a temporally uniform concentration, regardless of proximity to release sites, which is insufficient to activate low-affinity receptors (K_d = 1.2 μM; Richfield *et al*. 1989). In contrast, synchronous tonic firing would lead to spatially discrete concentrations that fluctuate with firing frequency. Note that the predicted basal dopamine level from asynchronous tonic firing is 30 nM, a value that is in the range of basal concentrations measured by microdialysis (Justice 1993). The actual value of the steady-state concentration from tonic firing will depend on the number of active dopaminergic neurons (Dai and Tepper 1998). In addition, our predictions only account for dopamine released by impulses; dopamine released by local factors such as activation of glutamate receptors might lead to higher basal concentrations (Kulagina *et al*. 2001).

We were especially interested in determining how cocaine, a drug of abuse, would alter the spatial profile of dopamine. For tonic firing, there was a general increase in dopamine levels owing to reduced uptake, but little change in the dopamine spatial profile. The magnitude of the simulated change in basal dopamine levels after cocaine agrees well with microdialysis results in which a fourfold increase was detected with the same dose (Kuczenski *et al*. 1991). However, for phasic firing, the dopamine concentration profile at longer times becomes more uniform after uptake inhibition, regardless of spatial heterogeneity. In this way, uptake inhibition increases dopaminergic control of the striatum by expanding the area over which a single dopaminergic terminal or a cluster of terminals acts.

These simulations show that there is a considerable difference in the concentration profiles elicited by tonic and phasic firing. Phasic firing elicits a temporally and spatially heterogeneous dopamine transient, which is rapidly dissipated owing to large concentration gradients. Thus, under phasic conditions, dopamine concentrations are poorly buffered. In contrast, during asynchronous tonic firing there is a temporally and spatially uniform concentration, i.e. it appears buffered, because there is a constant replenishing of dopamine. Concentration buffering has been suggested based on anatomical analysis (Pickel *et al*. 2002), and these results demonstrate that buffering depends on the activity state of firing.

While this paper was under review, a paper appeared by Floresco *et al*. (2003) that supports our findings. They showed that microdialysis sampling of dopamine release from nucleus accumbens terminals was not enhanced by burst firing unless an uptake inhibitor was introduced through the probe. Dopamine released by phasic firing in a heterogeneous environment leads to concentration gradients in which dopamine is diminished over short distances, a condition not found during asynchronous tonic firing (Fig. 6). These gradients restrict the concentration of dopamine that reaches a remote sensor, and they are diminished by uptake inhibition. This was recognized by the authors and interpreted as a failure of phasic release to diffuse out of the synapse unless uptake sites were blocked. Our quantitative treatment of the interplay between release, uptake and diffusion refine this interpretation by demonstrating that the relevant diffusion distances are 5–10 μm, much larger than the synaptic dimensions. Consistent with such expectations, an electrode located adjacent to a microdialysis probe reveals these concentration gradients and their removal by dopamine uptake inhibition (Yang *et al*. 1998).

Conclusion

This work clarifies the effects of phasic and tonic dopaminergic cell activity on volume transmission. The model decodes *in vivo* amperometric measurements of electrically evoked dopamine to provide rate constants for release and uptake as well as the extent of diffusion. The decoded rate constants allow prediction of how spatial heterogeneity of dopamine release and uptake sites affects dopamine concentration fluctuations during different activity states in the intact brain. Synchronous phasic firing can produce spatially and temporally heterogeneous concentration profiles whereas asynchronous tonic firing elicits uniform, steady-state dopamine concentrations.

Acknowledgements

This work was funded by NIH grants NS 15841 to RMW, DA 07418 to DS and NS 35298 to PAG. We thank Drs Regina Carelli and Donita Robinson for helpful discussion.

References

Allen C., Peters J. L., Sesack S. and Michael A. C. (2001) Microelectrodes closely approach intact nerve terminals *in vivo*, while larger devices do not: a study using electrochemistry and electron microscopy, in *Monitoring Molecules in Neuroscience: Proceedings of the 9th Conference on in Vivo Methods* (O'Connor W. T., Lowry J. P., O'Connor J. J. and O'Neill, R. D., eds), pp. 89–90. University College Dublin, Dublin.

Bath B. D., Michael D. J., Trafton B. J., Joseph J. D., Runnels P. L. and Wightman R. M. (2000) Subsecond adsorption and desorption of dopamine at carbon-fiber microelectrodes. *Anal. Chem.* **72**, 5994–6002.

Cahill P. S., Walker Q. D., Finnegan J. M., Mickelson G. E., Travis E. R. and Wightman R. M. (1996) Microelectrodes for the measurement of catecholamines in biological systems. *Anal. Chem.* **68**, 3180–3186.

Clapp-Lilly K. L., Roberts R. C., Duffy L. K., Irons K. P., Hu Y. and Drew K. L. (1999) An ultrastructural analysis of tissue surrounding a microdialysis probe. *J. Neurosci. Meth.* **90**, 129–142.

Cragg S. J., Nicholson C., Kume-Kick J., Tao L. and Rice M. E. (2001) Dopamine-mediated volume transmission in midbrain is regulated by distinct extracellular geometry and uptake. *J. Neurophysiol.* **85**, 1761–1771.

Dai M. and Tepper J. M. (1998) Do silent dopaminergic neurons exist in rat substantia nigra *in vivo*? *Neuroscience* **85**, 1089–1099.

Dayton M. A., Ewing A. G. and Wightman R. M. (1980) Response of microvoltammetric electrodes to homogeneous catalytic and slow heterogeneous charge-transfer reactions. *Anal. Chem.* **52**, 2392–2396.

Doucet G., Descarries L. and Garcia S. (1986) Quantification of the dopamine innervation in adult rat neostriatum. *Neuroscience* **19**, 427–445.

Dugast C., Suaud-Chagny M. F. and Gonon F. (1994) Continuous *in vivo* monitoring of evoked dopamine release in the rat nucleus accumbens by amperometry. *Neuroscience* **62**, 647–654.

Fallon J. H. and Moore R. Y. (1978) Catecholamine innervation of the basal forebrain. IV. Topography of the dopamine projection to the basal forebrain and neostriatum. *J. Comp. Neurol.* **180**, 545–580.

Floresco S. B., West A. R., Ash B., Moore H. and Grace A. A. (2003) Afferent modulation of dopamine neuron firing differentially regulates tonic and phasic dopamine transmission. *Nat. Neurosci.* **6**, 968–973.

Garris P. A. and Wightman R. M. (1994a) Different kinetics govern dopaminergic transmission in the amygdala, prefrontal cortex, and striatum: an *in vivo* voltammetric study. *J. Neurosci.* **14**, 442–450.

Garris P. A. and Wightman R. M. (1994b) *In vivo* voltammetric measurement of evoked extracellular dopamine in the rat basolateral amygdaloid nucleus. *J. Physiol.* **478**, 239–249.

Garris P. A., Ciolkowski E. L., Pastore P. and Wightman R. M. (1994) Efflux of dopamine from the synaptic cleft in the nucleus accumbens of the rat brain. *J. Neurosci.* **14**, 6084–6093.

Gerfen C. R. (1992) The neostriatal mosaic: multiple levels of compartmental organization. *Trends Neurosci.* **15**, 133–139.

Gonon F., Burie J. B., Jaber M., Benoit-Marand M., Dumartin B. and Bloch B. (2000) Geometry and kinetics of dopaminergic transmission in the rat striatum and in mice lacking the dopamine transporter, in *Progress in Brain Research* (Agnati L. F., Fuxe K., Nicholson C. and Sykova E., eds), pp. 291–302. Elsevier, Amsterdam.

Grace A. A. (1995) The tonic/phasic model of dopamine system regulation: its relevance for understanding how stimulant abuse can alter basal ganglia function. *Drug Alcohol Depend.* **37**, 111–129.

Grace A. A. and Bunney B. S. (1983) Intracellular and extracellular electrophysiology of nigral dopaminergic neurons – 3. Evidence for electrotonic coupling. *Neuroscience* **10**, 333–348.

Grace A. A. and Bunney B. S. (1984) The control of firing pattern in nigral dopamine neurons: single spike firing. *J. Neurosci.* **4**, 2866–2876.

Graybiel A. M. (1990) Neurotransmitters and neuromodulators in the basal ganglia. *Trends Neurosci.* **13**, 244–254.

Hyland B. I., Reynolds J. N. J., Hay J., Perk C. G. and Miller R. (2002) Firing modes of midbrain dopamine cells in the freely moving rat. *Neuroscience* **114**, 475–492.

Jones S. R., Garris P. A., Kilts C. D. and Wightman R. M. (1995) Comparison of dopamine uptake in the basolateral amygdaloid nucleus, caudate–putamen, and nucleus accumbens of the rat. *J. Neurochem.* **64**, 2581–2589.

Jones S. R., Joseph J. D., Barak L. S., Caron M. G. and Wightman R. M. (1999) Dopamine neuronal transport kinetics and effects of amphetamine. *J. Neurochem.* **73**, 2406–2414.

Justice J. B. Jr (1993) Quantitative microdialysis of neurotransmitters. *J. Neurosci. Meth.* **48**, 263–276.

Kristensen E. W., Wilson R. W. and Wightman R. M. (1986) Dispersion in flow injection analysis measured with microvoltammetric electrodes. *Anal. Chem.* **58**, 986–988.

Kuczenski R., Segal D. S. and Aizenstein M. L. (1991) Amphetamine, cocaine, and fencamfamine: relationship between locomotor and stereotypy response profiles and caudate and accumbens dopamine dynamics. *J. Neurosci.* **11**, 2703–2712.

Kuhr W. G., Wightman R. M. and Rebec G. V. (1987) Dopaminergic neurons: simultaneous measurements of dopamine release and single-unit activity during stimulation of the medial forebrain bundle. *Brain Res.* **418**, 122–128.

Kulagina N. V., Zigmond M. J. and Michael A. C. (2001) Glutamate regulates the spontaneous and evoked release of dopamine in the rat striatum. *Neuroscience* **102**, 121–128.

Michael D. J., Joseph J. D., Kilpatrick M. R., Travis E. R. and Wightman R. M. (1999) Improving data acquisition for fast-scan cyclic voltammetry. *Anal. Chem.* **71**, 3941–3947.

Michael A. C. and Wightman R. M. (1996) Microelectrodes, in: *Laboratory Techniques in Electroanalytical Chemistry* (Heineman W. R. and Kissinger P. T., eds), pp. 367–402. Marcel Dekker, New York.

Near J. A., Bigelow J. C. and Wightman R. M. (1988) Comparison of uptake of dopamine in rat striatal chopped tissue and synaptosomes. *J. Pharmacol. Exp. Ther.* **245**, 921–927.

Nicholson C. (1995) Interaction between diffusion and Michaelis–Menten uptake of dopamine after iontophoresis in striatum. *Biophys. J.* **68**, 1699–1715.

Nirenberg M. J., Vaughan R. A., Uhl G. R., Kuhar M. J. and Pickel V. M. (1996) The dopamine transporter is localized to dendritic and axonal plasma membranes of nigrostriatal dopaminergic neurons. *J. Neurosci.* **16**, 436–447.

Paxinos G. and Watson C. (1986) *The Rat Brain in Stereotaxic Coordinates*. Academic, New York.

Peters J. L. and Michael A. C. (2000) Changes in the kinetics of dopamine release and uptake have differential effects on the spatial distribution of extracellular dopamine concentration in rat striatum. *J. Neurochem.* **74**, 1563–1573.

Phillips P. E. M., Stuber G. D., Heien M. L. A. V., Wightman R. M. and Carelli R. M. (2003) Subsecond dopamine release triggers cocaine seeking. *Nature* **422**, 614–618.

Pickel V. M., Garzon M. and Mengual E. (2002) Electron microscopic immunolabeling of transporters and receptors identifies transmitter-specific functional sites envisioned in Cajal's neuron, in *Progress in Brain Research* (Azmitia E. C., DeFelipe J., Jones E. G., Rakic P. and Ribak C. E., eds), pp. 145–155. Elsevier, Amsterdam.

Pierce R. C. and Rebec G. V. (1990) Stimulation of both D1 and D2 dopamine receptors increases behavioral activation and ascorbate release in the neostriatum of freely moving rats. *Eur. J. Pharmacol.* **191**, 295–302.

Richfield E. K., Penney J. B. and Young A. B. (1989) Anatomical and affinity state comparisons between dopamine D1 and D2 receptors in the rat central nervous system. *Neuroscience* **30**, 767–777.

Robinson D. L., Phillips P. E. M., Budygin E. A., Trafton B. J., Garris P. A. and Wightman R. M. (2001) Sub-second transient

dopamine release in the nucleus accumbens of sexually behaving rats. *Neuroreport* **12**, 2549–2552.
Robinson D. L., Heien M. L. A. V. and Wightman R. M. (2002) Frequency of dopamine concentration transients increases in dorsal and ventral striatum of male rats during introduction of conspecifics. *J. Neurosci.* **22**, 10477–10486.
Schmitz Y., Lee C. J., Schmauss C., Gonon F. and Sulzer D. (2001) Amphetamine distorts stimulation-dependent dopamine overflow: effects on D2 autoreceptors, transporters, and synaptic vesicle stores. *J. Neurosci.* **21**, 5916–5924.
Schönfuß D., Reum T., Olshausen P., Fischer T. and Morgenstern R. (2001) Modelling constant potential amperometry for investigations of dopaminergic neurotransmission kinetics *in vivo*. *J. Neurosci. Meth.* **112**, 163–172.
Schultz W. (1986) Responses of midbrain dopamine neurons to behavioral trigger stimuli in the monkey. *J. Neurophysiol.* **56**, 1439–1461.
Schultz W. (1998) Predictive reward signal of dopamine neurons. *J. Neurophysiol.* **80**, 1–27.
Sesack S. R., Aoki C. and Pickel V. M. (1994) Ultrastructural localization of D2 receptor-like immunoreactivity in midbrain dopamine neurons and their striatal targets. *J. Neurosci.* **14**, 88–106.
Suaud-Chagny M. F., Dugast C., Chergui K., Msghina M. and Gonon F. (1995) Uptake of dopamine released by impulse flow in the rat mesolimbic and striatal systems *in vivo*. *J. Neurochem.* **65**, 2603–2611.
Venton B. J., Troyer K. P. and Wightman R. M. (2002) Response times of carbon-fiber microelectrodes to dynamic changes in catecholamine concentration. *Anal. Chem.* **74**, 539–546.
Vizi E. S. (2000) Role of high-affinity receptors and membrane transporters in nonsynaptic communication and drug action in the central nervous system. *Pharmacol. Rev.* **52**, 63–89.
Wightman R. M. and Robinson D. L. (2002) Transient changes in mesolimbic dopamine and their association with reward. *J. Neurochem.* **82**, 721–735.
Wightman R. M. and Zimmerman J. B. (1990) Control of dopamine extracellular concentration in rat striatum by impulse flow and uptake. *Brain Res. Brain Res. Rev.* **15**, 135–144.
Yang H., Peters J. L. and Michael A. C. (1998) Coupled effects of mass transfer and uptake kinetics on *in vivo* microdialysis of dopamine. *J. Neurochem.* **71**, 684–692.
Zoli M., Torri C., Ferrari R., Jansson A., Zini I., Fuxe K. and Agnati L. F. (1998) The emergence of the volume transmission concept. *Brain Res. Brain Res. Rev.* **26**, 136–147.

Supplementary Material Figure Legend

The movie shows the dopamine concentrations elicited by tonic, asynchronous firing of dopamine neurons at 5 Hz and then a four-pulse, 20 Hz burst. Release and uptake sites are determined as in Fig. 6, with green sections containing both release and uptake sites, and dark (non-green) sections containing neither. The burst occurs at 0.4 s.

Appendix

Theory of finite-difference model

Conditions governing dopamine uptake, release and diffusion

The instantaneous dopamine concentration in the extracellular space is determined by the rates of release, uptake and mass transport (Nicholson 1995). In this paper, the kinetics of dopamine release and uptake in the brain extracellular fluid were described by previously established equations (Wightman and Zimmerman 1990; Nicholson 1995). Release was characterized by a fixed concentration ($[DA]_p$) that appears adjacent to a release site immediately with each impulse in a stimulation train. Dopamine uptake was described by Michaelis–Menten kinetics:

$$\left(\frac{d[\mathrm{DA}]}{dt}\right)_{uptake} = \frac{-V_{\max}[\mathrm{DA}]}{K_m + [\mathrm{DA}]} \quad (1)$$

where V_{max} is the maximal rate of uptake by the transporter and K_m is the affinity of the transporter for dopamine. $[DA]_p$ and V_{max} are defined in terms of the volume of the extracellular space (20% of the tissue volume). Mass transport was considered diffusional and was described by Fick's second law, which for planar diffusion is:

$$\left(\frac{d[\mathrm{DA}]}{dt}\right)_{diffusion} = D\frac{d^2[\mathrm{DA}]}{dx^2} \quad (2)$$

The diffusion coefficient for dopamine (D) in this space was assumed to be 2×10^{-6} cm^2/s (Nicholson 1995), which accounts for the measured tortuosity.

Concentration gradients arise from the heterogeneous distribution of release sites. These geometrical distributions provide boundary conditions to obtain solutions to the differential equations. We considered the following cases:

(i) *Diffusion to a cylindrical carbon-fiber electrode operated in the amperometric mode.* The dopamine concentration was initially taken to be zero, and release and uptake sites were assumed to be continuous. This approximates the close spacing of dopamine terminals (Doucet *et al*. 1986). The local concentration was increased by $[DA]_p$ with each stimulation pulse and was removed according to Michaelis–Menten kinetics (Wightman and Zimmerman 1990). The concentration at the electrode surface was maintained at zero to model amperometry.

To this point, the model is quite similar to those of Schmitz *et al*. (2001) and Schönfuß *et al*. (2001). However, two modifications were made. First, the catalytic reaction of ascorbate, which is present in high concentrations in the brain, was added to the simulation. The amperometric oxidation of dopamine generates DOQ that can diffuse away from the electrode and be reduced back to dopamine by ascorbate. The catalytic regeneration of dopamine is a second-order reaction:

$$\left(\frac{d[\mathrm{DA}]}{dt}\right)_{catalytic} = k^*[\mathrm{AA}]^*[\mathrm{DOQ}] \quad (3)$$

where k is 3.2×10^5 M^{-1} s^{-1} (Dayton *et al*. 1980) and [AA] is the brain extracellular ascorbate concentration (600 μM; Venton *et al*. 2002).

Second, we relate flux (J), the measured quantity in amperometry, to concentration. The amperometric current was calculated from Fick's first law:

$$J = -D\frac{d[\mathrm{DA}]}{dx} = \frac{i}{nFA} \tag{4}$$

where i is the current, n is the number of electrons transferred, F is Faraday's constant and A is the electrode area (typically 900 μm^2). Instead of planar diffusion as used in Schmitz *et al*. (2001), the electrochemical simulator employed cylindrical coordinates (as in Schönfuß *et al*. 2001).

(ii) *Diffusion in the extracellular space between release sites.* Diffusional contributions in the absence of an electrode were simulated. Spatially discrete release and uptake sites were arranged based on histological data in a single dimension (see Results) and were assumed to follow identical kinetic behavior as in the simulations described above. To mimic synchronous firing, dopamine concentrations throughout the simulation space were raised simultaneously at the time of an action potential. During simulations of continuous, asynchronous firing, neurons were simulated to fire independently of each other at an average rate of 5 Hz by using a random number generator to determine when release events occured.

Finite-difference computation of amperometric data

To solve the differential equations a finite-difference method was used. A one-dimensional finite-difference model for dopamine uptake and release during amperometry has been described (Schmitz *et al*. 2001).

We tracked the concentration of dopamine in various distance bins away from the electrode for a series of time steps (Δt), based on the equation

$$\Delta t = \frac{\Delta r^2}{2D} \tag{5}$$

where Δr is the size of the bin and D is the appropriate diffusion coefficient. Bin lengths were small (0.5 μm), so the concentrations were evaluated at intervals less than 0.5 ms. If a bin contained a release site, it instantly received $[\mathrm{DA}]_\mathrm{p}$ when a stimulation pulse occured. The change in dopamine concentration due to planar diffusion over a time step for bin j ($\Delta\mathrm{DA}_{diffusion}$) was given by the finite-difference notation for equation 2:

$$\Delta\mathrm{DA}_{diffusion} = \frac{1}{2}\mathrm{DA}_{j-1} + \frac{1}{2}\mathrm{DA}_{j+1} - \mathrm{DA}_j \tag{6}$$

where DA_{j+1} and DA_{j-1} are the dopamine concentrations in the neighboring bins on the previous time step. To simulate amperometric data, cylindrical coordinates were used and the change in concentration for bin j was given by (Michael and Wightman 1996):

$$\Delta\mathrm{DA}_{diffusion} = \frac{j}{(2j-1)}\mathrm{DA}_{i+1} + \frac{(j-1)}{(2j-1)}\mathrm{DA}_{j-1} - \mathrm{DA}_j \tag{7}$$

Dopamine uptake was computed with the finite-difference version of equation 1

$$\Delta\mathrm{DA}_{uptake} = \frac{V_\mathrm{max}[\mathrm{DA}]}{K_\mathrm{m} + [\mathrm{DA}]}\Delta t \tag{8}$$

The dopamine concentration was modeled over a distance extending 200 μm from the electrode to prevent the location of the outer boundary from affecting the results. Simulations were smoothed with a four-point moving average. Because the time steps were small, this causes minimal effects on the temporal accuracy of the model.

At the electrode, DOQ is formed according to the following equation

$$\mathrm{DA} - 2e^- \rightarrow \mathrm{DOQ} + 2\mathrm{H}^+ \tag{9}$$

The diffusion coefficient of DOQ was assumed to be equal to that of dopamine and DOQ was assumed to diffuse following the same equations as dopamine. On each time step, some DOQ is converted back to dopamine. The finite-difference notation for the catalytic reaction in equation 3 is:

$$\Delta\mathrm{DA}_{catalytic} = k^*[\mathrm{AA}]^*[\mathrm{DOQ}]^*\Delta t \tag{10}$$

The final concentration of dopamine ($\Delta\mathrm{DA}_{final}$) in each bin was given by

$$\Delta\mathrm{DA}_{final} = \Delta\mathrm{DA}_{diffusion} + \Delta\mathrm{DA}_{catalytic} - \Delta\mathrm{DA}_{uptake} \tag{11}$$

The finite-difference calculation of the flux at the electrode surface as current (i) was given by:

$$i = \Delta\mathrm{DA}_{final} \times \frac{nFAD}{\Delta r} \tag{12}$$

where $\Delta\mathrm{DA}_{final}$ is the concentration in the bin next to the electrode.

Tests of the finite-difference model

Simulations of amperometry were identical to those of Schmitz *et al*. (2001) when their boundary conditions were used. Because the computed dopamine concentrations in each bin are quite small, the finite-difference model was also compared with the results of a random walk simulation of dopamine diffusion, release and uptake with first-order kinetics (data not shown). Both simulations yielded similar results. We prefer the finite-difference approach because it requires less computation to produce an acceptable trace and the calculation of Michaelis–Menten chemical kinetics is more straightforward.